Canada at 5,000 yr BP would produce warmer and moister summer conditions. A southward shift following 4,000 yr BP would cause a return to dominance by cool dry arctic air.

The earliest indications of the transition from tundra to forest-tundra vegetation and changes in lake characteristics are coincidental changes in the pollen and diatom percentages from the Queen's Lake core (Fig. 1). For the period 5,600–3,820 yr BP the time interval represented by 2.5 cm of deposition between each pollen and diatom sample is ~150 years. The shift in diatom flora from an acidophilous, low productivity assemblage to an assemblage reflecting higher pH and productivity occurs at exactly the same time as the shift in the pollen percentages. However, the shifts in total lake productivity as measured by diatom valve concentration, LOI and $\delta^{13}C$, and the geochemical and hydrological conditions of the lake as measured by elemental geochemistry and $\delta^{18}O$ were 150–300 years slower in registering a response to the shift from tundra to forest-tundra environmental conditions (Fig. 1). This suggests that the composition of the diatom flora adjusted quickly to temperature changes whereas adjustments of the total lake productivity and isotope balance took longer. Rapid change in small lakes, particularly in the composition of the diatom flora, is not surprising as short life cycles and widespread dispersal ability allow diatoms to respond quickly to changes in climate[20]. Surprisingly, the record from Queen's Lake, and the information from the other sites, does not indicate a large time lag between changes in lake characteristics and changes in treeline vegetation (Figs 1 and 2). The rapid increase in *Picea mariana* at Queen's Lake may have been helped by its typical spatial distribution in central Canada, where scattered krummholz occur more than 100 km north of the mapped limits of forest-tundra. Intervals of mild climate as short as 10 years have been shown to initiate successful reproduction by treeline populations of *Picea* in eastern Canada[21]. Scattered trees that can rapidly produce viable seeds at the onset of climate warming provide ideal expansion foci which promote fast responses to favourable environmental changes[22]. The rapid changes in vegetation and lake characteristics at 5,000 yr BP may reflect rapid and synchronous climatic warming. It is also possible the nonlinear ecological responses caused by feedbacks between vegetation, permafrost, soils and boundary-layer climate could amplify rates of vegetation and lake ecosystem change once critical thresholds are crossed[5].

Our evidence on the nature and rate of past environmental changes at treeline may help to predict the response of vegetation, hydrology and lake characteristics to future climate warming. These results show that for the central Canadian treeline, the 250-year time frame used in modelling the short-term response of northern boreal forests is reasonable[5,6]. Palaeoecological investigations of *Pinus sylvestris* treeline in northern Scotland suggest similar rapid responses of vegetation and hydrology to shifts in the Azores high between 4,400 and 3,800 yr BP[23]. The rapid change in the distribution of *Pinus sylvestris* may not have required the same spatial distribution of seed sources as we propose for *Picea mariana* in central Canada. Late Holocene episodes of climate change such as these in central Canada and Scotland may be better analogues for future global warming than is the change from glacial to nonglacial conditions, when the distribution of solar radiation and Earth boundary conditions were very different from today[24]. It remains a concern that greenhouse warming may occur even faster than these Holocene events[23]. □

Received 26 October; accepted 8 December 1992.

1. Schlesinger, M. E. & Mitchell, J. F. B. *Rev. Geophys.* **25,** 760–798 (1989).
2. BOREAS Science Steering Committee. *Eos* **72,** 33–35 (1990).
3. Wilson, M. F., Henderson-Sellers, A., Dickinson, R. E. & Kennedy, P. J. *J. Clim.* **7,** 319–343 (1987).
4. Bonan, G. B., Pollard, D. & Thompson, S. L. *Nature* **359,** 716–718 (1992).
5. Pastor, J. & Post, W. M. *Nature* **334,** 55–58 (1988).
6. Bonan, G. B., Shugart, H. H. & Urban, D. L. *Clim. Change* **16,** 9–29 (1990).
7. Ritchie, J. C., Cwynar, L. C. & Spear, R. W. *Nature* **305,** 126–128 (1983).
8. Moser, K. A. & MacDonald, G. M. *Quat. Res.* **34,** 227–239 (1990).
9. Dyke, A. S. & Prest, V. K. *Geog. phys. Quat.* **41,** 237–264 (1987).
10. Ecoregions Working Group *Ecoclimatic Regions of Canada, First Approximation* (Ecological Land Classification Series No. 23, Environment Canada, Ottawa, 1989).
11. Ryan, D. F. & Kohler, D. M. *Limnol. Oceanogr.* **32,** 751–757 (1987).
12. Rosenberg, I., Korsman, T. & Anderson, N. J. *Phil. Trans. R. Soc. Lond.* B**327,** 371–372 (1990).
13. Jones, B. F. & Bowser, C. J. in *Lakes–Chemistry, Geology, Physics* (ed. Lerman, A.) 179–235 (Springer, New York, 1978).
14. Talbot, M. R. *Chem. Geol. (Isotope Geosci.)* **80,** 261–279 (1990).
15. Bursey, G. G., Edwards, T. W. D. & Frape, S. K. in *Northern Hydrology: Selected Perspectives* (eds Prowse, T. D. & Ommanney, C. S. L.) 17–31 (NHRI Symp. No. 6, Environment Candada, Saskatoon, 1991).
16. Lafleur, P. M., Rouse, W. R. & Carlson, D. W. *Int. J. Clim.* **12,** 193–203 (1992).
17. Kay, P. A. *Quat. Res.* **11,** 125–140.
18. Sorenson, C. J. *Ann. Am. Assoc. Geog.* **67,** 214–222 (1977).
19. Ritchie, J. C. & Hare, F. K. *Quat. Res.* **1,** 331–341 (1971).
20. Smol, J. P., Walker, I. R. & Leavitt, P. R. *Verh. int. Verein. Limnol.* **24,** 1240–1246 (1991).
21. Payette, S., Filion, L., Gauthier, L. & Boutin, Y. *Nature* **315,** 135–138 (1985).
22. Carter, R. N. & Prince, S. D. *Nature* **293,** 644–645 (1981).
23. Gear, A. J. & Huntley, B. *Science* **251,** 544–547 (1991).
24. Kutzbach, J. E. & Guetter, P. J. *J. atmos. Sci.* **43,** 1726–1759 (1986).
25. Faegri, K. & Iversen, J. *Textbook of Pollen Analysis*, 3rd edn (Munksgaard, Copenhagen, 1975).
26. Smol, J. P. *Can. J. Bot.* **61,** 2195–2204 (1983).
27. Smol, J. P. *Hydrobiologia* **123,** 199–208 (1985).
28. Dean W. E. *J. Sedim. Petrol.* **44,** 242–248 (1974).
29. Muecke, G. K. *A Short Course in Neutron Activation Analysis in the Geosciences* (Mineralogical Association of Canada, Toronto, 1980).
30. MacDonald, G. M., Larsen, C. P. S., Szeicz, J. M. & Moser, K. A. *Quat. Sci. Rev.* **10,** 53–71 (1991).
31. Edwards, T. W. D. & McAndrews, J. H. *Can. J. Earth Sci.* **26,** 1850–1859 (1989).
32. Thompson, P. & Gray, J. *Int. J. appl. Radiation Isotopes* **28,** 411–415 (1977).
33. Edwards, T. W. D. in *Continental Isotopic Indicators of Climate* (eds Swart, P. K., McKenzie, J. A. & Lohmann, K. C.) (AGU, Washington DC, in the press).

ACKNOWLEDGEMENTS. This research was supported by NSERC and the NSTP. The paper benefited from comments by J. Pastor.

Origin of modal and rhythmic igneous layering by sedimentation in a convecting magma chamber

R. Stephen Sparks*, Herbert E. Huppert†, Takehiro Koyaguchi‡ & Mark A. Hallworth†

* Department of Geology, University of Bristol, Bristol BS8 1RJ, UK
† Institute of Theoretical Geophysics, University of Cambridge, Cambridge CB3 9EW, UK
‡ Earthquake Research Institute University of Tokyo, Tokyo 13, Japan

EXPERIMENTAL investigations of convecting, particle-laden fluids show two regimes for convection driven by cooling from above[1]. In very dilute suspensions, convection will maintain a homogeneous distribution of particles throughout the convecting layer provided that particle fall velocities are small compared with turbulent fluid velocities. Above a critical concentration, convection is unable to keep the particles suspended, so the particles settle, leaving behind a layer of convecting fluid virtually free of particles. Here we apply these results to cooling magma chambers, in which crystallization leads to an increase in suspended crystal content with time. Discrete sedimentation events are predicted each time the concentration exceeds the critical value. For common igneous minerals, critical concentrations are very small (typically 0.002–0.03 wt%) and layers of the order of centimetres to a few metres thick will result. Because minerals of different density and size have different critical concentrations and settling velocities, complex fluctuations in sedimentation rate and mineral proportions can occur in a multi-component melt. This may lead to either regular repetitive cycles or more complex fluctuations. The process is confined to low-viscosity magmas, such as basalts, in which the crystals are able to separate from the active thermal boundary layer during convection.

The concepts of crystal settling and convection in magma chambers have a long history[2–6]. Wager and co-workers[5,6] were struck by the strong resemblance of layered igneous rocks in the Skaergaard intrusion to clastic sedimentary rocks. Observations of graded bedding, trough structures and cross-layering

suggested sedimentation from magmatic currents induced either by convection[6] or by gravity currents[7].

There have been doubts as to whether crystal settling can explain layering[8,9]. Other mechanisms for layering have been recognized; these include *in situ* crystallization[8], kinetic effects of crystal nucleation and growth[10,11], and double-diffusive layered convection[8,9,12]. Experimental and theoretical studies[1,13,14] of convecting suspensions heated from below show, however, that settling can occur at the base of a suspension even if the convection maintains a uniform concentration. Petrological observations[15] show excess feldspar in many basaltic lavas which is most easily explained by crystal settling. The alternative layering models do not provide entirely convincing explanations of the basic 'cumulus' textures of layered rocks which are most simply interpreted as a framework of settled individual grains[6]. The oriented and dendritic morphologies due to growth *in situ* are less commonly observed than the apparent packstone texture. The more strikingly 'sedimentary' structures such as layers graded by grain size or density, and cross-layering, are also simply explained by sedimentation. Here we extend the results of experiments on convection in a suspension cooled from above[1]. We propose a powerful mechanism for inducing the fluctuations in sedimentation rate and mineral proportions needed to cause much of the observed complexity in mesoscale modal and rhythmically layered rocks formed on the floors of magma chambers.

For our experiments we used a cubical tank of water seeded with silicon carbide grit of fairly uniform size, which was cooled uniformly from the top. This resulted in convection at high Rayleigh number ($Ra \approx 10^8$–10^9) with turbulent velocities at least two orders of magnitude greater than the settling velocities of the particles. For very dilute concentrations, the convection distributed the particles uniformly throughout the tank. Simultaneously, sedimentation occurred at the base, as in previous experiments[13], so the mean concentration decreased with time. However, above a critical concentration a sharp descending interface was observed between a convecting upper clear region and a non-convecting lower region in which there was unimpeded sedimentation by Stokes law. Warmer fluid escaped through the interfacial region above the sedimenting layer and enhanced the convection driven by cooling at the roof. The lower-layer temperature remained uniform during sedimentation, confirming that it was stagnant.

The two-layer structure will be stable only if the density of the cool, clear upper layer is less than the bulk density of the sedimenting lower layer. Expressing this concept quantitatively and analytically solving the differential equations for the heat budget of the two layers[1], we showed rigorously that the two regimes are separated by a critical concentration

$$C_* = \frac{\rho_p}{\rho_p - \rho_0}\alpha(T_0 - T_u) \qquad (1)$$

where ρ_0 is the density of the fluid at $T = T_0$, the constant temperature of the lower fluid layer, ρ_p is the particle density, α is the coefficient of thermal expansion of the fluid and T_u is the temperature of the upper fluid. The experimental observations[1] agree well with this criterion, especially when allowance is made for the transfer of small amounts of fine particles which are swept up into the upper convecting layer across the interface.

We now extend these concepts to combine the process of crystallization with the phenomena observed in the experiments, using inert particles to provide a general mechanism of layering (Fig. 1). We envisage a convecting magma chamber of height H, cooled from above. In addition there will be compositional convection from crystals at the floor[9]. Temperature decreases in the convecting interior. Suspended crystals form and are kept uniformly distributed within the interior. Concentration of crystals increases with time while some sedimentation from the suspension occurs on the floor[13]. The concentration of crystals reaches the critical value, as given by equation (1), and a discrete

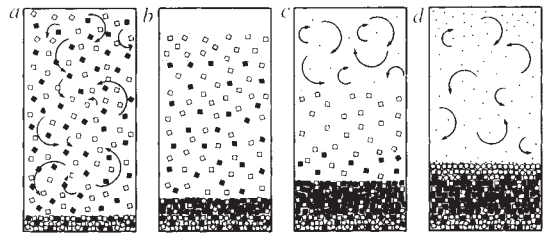

FIG. 1 Sequence of events in a magma chamber precipitating two phases of different size and density. *a*, Crystals are uniformly distributed through the chamber by convection. The interior cools, resulting in crystallization. Some sedimentation occurs at the chamber floor[13] but crystal concentration increases with time. *b*, Critical concentration (equation (1)) is reached and the suspended crystals sediment in a stagnant layer in which convection is dampened. *c*, Clear, crystal-free convection layer forms above the sedimenting layer which forms a density-graded layer. *d*, Cycle begins again with formation of new crystals in the convecting chamber. Some of the lower-density crystals are shown swept up into the convecting layer.

sedimentation event follows. As the lower layer sediments, the upper layer continues to cool and crystallization begins again. The timescale for sedimentation is H/v_S where v_S is the Stokes free-fall velocity; the timescale for cooling is H^2/κ, where κ is the thermal diffusivity[16]. If the ratio of these timescales, κ/Hv_S, is small, as is typically the case, these processes can be considered to occur sequentially. In the simplest case of one phase, a repetitive sequence of layers should form on the floor of the chamber. If the sedimenting layer had a range of crystal sizes a graded bed could form, thereby providing an alternative mechanism to magmatic density currents[7].

The thicknesses of the layers can be deduced from equation (1). Earlier studies, which equated the convective heat flux in the magma to the conductive heat flux through the solid overlying roof[16,17], indicate that the typical temperature differences driving convection in a magma chamber are 0.1–10 °C. Although these differences seem small, the resulting convective motions are sufficient to maintain crystals in suspension, except at the floor where sedimentation can occur[13]. Typical values of the relevant parameters are $\alpha = 5\times10^{-5}$ K^{-1}, $\rho_0 = 2{,}650$ kg m^{-3}, $\rho_p = 3{,}300$ kg m^{-3} for olivine and $\rho_p = 2{,}700$ kg m^{-3} for plagioclase. For $T_0 - T_u \approx 0.1$ °C, the critical concentration is 0.0025 wt% for olivine and 0.027 wt% for plagioclase. For a chamber 1 km deep, the thickness of the sediment layer formed from such a sedimentation pulse would be 4 cm for olivine and 50 cm for plagioclase, assuming a packing fraction of 50%. For larger values of $T_0 - T_u$ the layer thicknesses will increase in proportion. Clearly there are other choices for the parameters, but for all realistic values the critical concentrations will be small, and the length scale of the individual layers will be a small fraction of the chamber depth in the range of a few centimetres to several metres.

The mechanism allows for great variation and complexity in magma chamber sedimentation. Each mineral phase will have a different critical concentration. Substantial fluctuations in sedimentation rate and proportions of each phase would be expected. We now discuss examples seen in the field which illustrate these concepts.

In the Rhum intrusion, centimetre- to metre-scale layering occurs in troctolites. Detailed stratigraphic logging[18,19] reveals that the layering is largely caused by fluctuation in the size, shape and proportions of olivine surrounded by plagioclase. Average proportions of minerals are cotectic (70% plagioclase and 30% olivine), but these proportions fluctuate substantially from layer to layer. Although Rhum was an open-system chamber[18], systematic changes in the mineral compositions in layered troctolites[19,20,21] imply that the small-scale layering developed during periods of closed-system evolution. As olivine has a much lower critical concentration than plagioclase (see equation (1)), the scale of olivine layering should be smaller

than for plagioclase, as is observed. We envisage a convecting magma chamber precipitating olivine and plagioclase in cotectic proportions. When the concentration of crystals reaches a critical value, a sedimentating layer forms with the crystals settling at their Stokes fall velocities (Fig. 1). Olivine typically settles faster than plagioclase because of its greater density contrast with basaltic magma, so a layer of plagioclase is left behind (Fig. 1). If the plagioclase concentration is still less than critical for plagioclase alone, then the plagioclase would be mixed up into the 'clear layer' in the same way that in the experiments fine particles were swept up from the interfacial zone into the clear layer. Olivine and plagioclase continue to crystallize in the upper layer until critical concentrations are again reached and another pulse of sedimentation occurs. Eventually the critical concentration for plagioclase is achieved and the excess plagioclase is sedimented in a pulse generating anorthosite layers poor in olivine.

In the Skaergaard intrusion, one sees irregular modal layering, regular repetitions of graded beds (gravity stratification) and alternations of homogeneous gabbro cumulates and strongly density graded layers[5,6,22]. We postulate that the alternation of homogeneous gabbro and graded layers is produced by a magma chamber that remains below the critical concentration for substantial periods of time and generates a steady accumulation of crystals on the floor in the cotectic proportions. A graded bed represents a pulse of sedimentation whenever the critical concentration is attained. In this case the crystals in the chamber settle out according to size and density.

Many complex interactions can take place with the co-precipitation of two or more minerals of different density. For example, as a plagioclase-rich layer sediments, fast-settling olivine formed in the overlying layer can fall through the interfacial zone and the excess density flux can overturn the layer. Nonlinear crystal growth and nucleation rates and the sedimentation velocities are coupled together with the cooling rate imposed by convection, magma viscosity and phase relationships. Complex fluctuations in the sedimentation rates and modal proportions are possible. It is not surprising that a wide range of patterns can develop, from the complex layering of Rhum troctolites to the regularity in parts of the Skaergaard intrusion.

The proposed mechanism requires that crystals formed in the thermal boundary layer at the roof of the chamber can escape by settling before the boundary layer becomes unstable locally. This will occur if the viscosity of the magma is low enough for crystals to escape from the boundary layer on the convective timescale rather than remaining to contribute to the density evolution of the boundary layer. If, instead, the viscosity is high and crystals are maintained in the boundary layer, the crystal content and density of the thermal boundary layer will always exceed the density of the underlying warmer suspension and equation (1) is not valid. We can estimate when equation (1) will be applicable when crystals are growing in the boundary layer by an approximate analysis of local conditions. The mean thickness, δ, of the thermal boundary layer is given by[23]

$$\delta \approx (\mu\kappa R_c/\alpha\Delta T g\rho_0)^{1/3} \quad (2)$$

where R_c is the critical value of the Rayleigh number ($\sim 10^3$), μ is the magma viscosity, κ is the thermal diffusivity, α is the coefficient of thermal expansion, ΔT is the temperature difference driving convection, g is gravity and ρ_0 is the magma density. The timescale, τ, for the instability of the boundary layer to occur is given by the time taken for conduction to thicken the local boundary layer to this mean thickness

$$\tau \approx (\mu R_c/\alpha\Delta T\rho_0 g)^{2/3}\kappa^{-1/3} \quad (3)$$

The two different regimes can be separated by equating the settling time, ϕ/v_S to the convective boundary-layer timescale, τ. Using Stokes law for a crystal of diameter d and density contrast $\Delta\rho$ and equating (2) and (3), we find that the critical viscosity, μ_c, below which equation (1) is valid is

$$\mu_c \approx \left(\frac{g\Delta\rho d^2}{18}\right)^{3/2}\left(\frac{R_c\mu\kappa}{\alpha\Delta T g\rho_0}\right)^{1/2}\kappa^{-1} \quad (4)$$

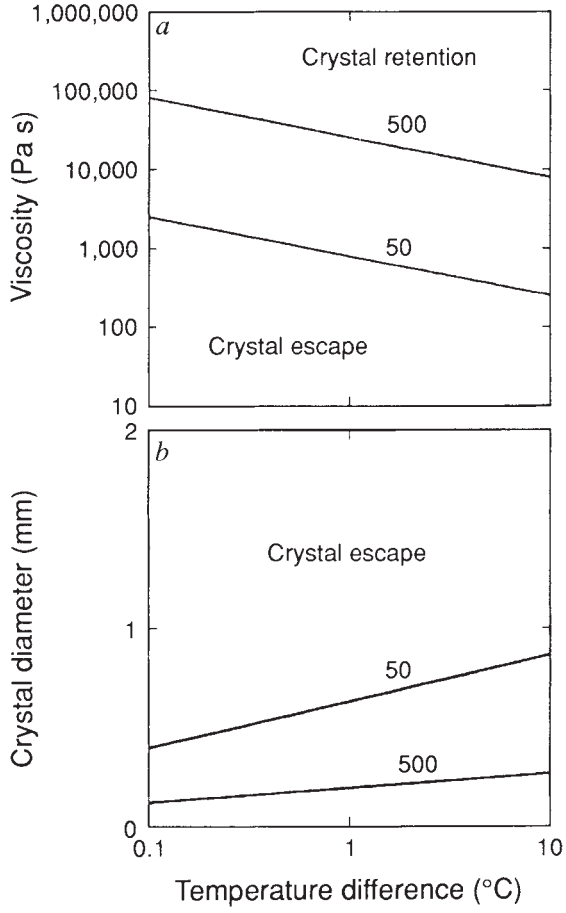

FIG. 2 *a*, Critical viscosity separating thermal boundary layers that retain crystals from those from which the crystals can escape is shown as a function of temperature difference driving convection. The lines show calculations for 5-mm-diameter crystals with density contrasts of 500 and 50 kg m^{-3} with the magma. Crystals can escape from sufficiently low-viscosity magmas before the thermal boundary layer destabilizes locally. *b*, Maximum crystal size that can be retained in the thermal boundary layer for a magma with viscosity 30 Pa s as a function of temperature difference driving convection. Calculations are shown for density differences between crystal and magma of 50 and 500 kg m^{-3}. The calculations indicate that crystals larger than 1 mm can usually escape from thermal boundary layers before they become unstable locally.

Figure 2*a* shows calculations of μ_c as a function of temperature differences in the range 0.1–10 °C for crystals of diameter 5 mm and density contrasts of 50 and 500 kg m^{-3}. The temperature range covers typical values expected in magma chambers. Figure 2*b* shows the crystal size that must be exceeded for crystals to escape from the thermal boundary layer for a magma with viscosity of 30 Pa s, this being typical for basalt. We conclude that the mechanism will be effective in low-viscosity basic and intermediate magmas and can occur in basaltic magmas for crystals of diameter $\geq$1 mm. The absence of layering in rocks formed from viscous magmas is consistent with the rheological control implied by our analysis. Appropriate conditions for layering by the mechanism proposed here only occur when crystals escape from the unstable boundary layer or crystal nucleation occurs in the interior[11]. □

Received 10 August; accepted 21 December 1992.

1. Koyaguchi, T., Hallworth, M. A. & Huppert, H. E. *J. Volcanol. geotherm. Res.* (in the press).
2. Darwin, C. R. *Second Part of the Geology of the Voyage of the Beagle* (London, 1844).

3. Lewis, J. V. *N. J. Geol. Surv.* **11,** 99–153 (1907).
4. Bowen, N. L. *Am. J. Sci.* **39,** 175–191 (1915).
5. Wager, L. R. & Deer, W. A. *Meddr. Gronland* **105,** 1–32 (1939).
6. Wager, L. R. & Brown, G. M. *Layered Igneous Rocks* (Oliver & Boyd, Edinburgh, 1968).
7. Irvine, T. N. *Am. J. Sci.* **A280,** 1–58 (1980).
8. McBirney, A. R. & Noyes, R. M. *J. Petrol.* **20,** 485–554 (1979).
9. Sparks, R. S. J., Huppert, H. E. & Turner, J. S. *Phil. Trans. R. Soc. Lond.* **A310,** 511–534 (1984).
10. Morse, S. A. *Mem. Geol. Soc. Am.* **112** (1969).
11. Brandeis, G. & Jaupart, C. *Earth planet Sci. Lett.* **77,** 345–361 (1986).
12. Turner, J. S. *Nature* **285,** 213–215 (1980).
13. Martin, D. & Nokes, R. *Nature* **332,** 534–536 (1988).
14. Koyaguchi, T., Hallworth, M. A., Huppert, H. E. & Sparks, R. S. J. *Nature* **343,** 447–450 (1990).
15. Cox, K. G. & Mitchell, C. *Nature* **333,** 447–449 (1988).
16. Huppert, H. E. & Sparks, R. S. J. *J. Fluid Mech.* **188,** 107–131 (1988).
17. Worster, M. G., Huppert, H. E. & Sparks, R. S. J. *Earth planet Sci. Lett.* **101,** 78–79 (1990).
18. Brown, G. M. *Phil. Trans. R. Soc. Lond.* **B240,** 1–53 (1956).
19. Bedard, J. H. J., Sparks, R. S. J., Renner, R., Cheadle, M. J. & Hallworth, M. A. *J. geol. Soc. Lond.* **145,** 204–207.
20. Tait, S. R. *Geol. Mag.* **122,** 469–484 (1985).
21. Dunham, A. C. & Wadsworth, W. J. *Miner. Mag.* **42,** 347–356 (1978).
22. Maaloe, S. *Origins of Igneous Layering* ed. Parsons, I. 247–262 (Reidel, 1986).
23. Howard, L. N. *Proc. 11th int. Congress appl. Mech* 1109–1115 (1964).

ACKNOWLEDGEMENTS. We acknowledge support from Venture Research International and a thoughtful review from Claude Jaupart.

Carbon dioxide limitation of marine phytoplankton growth rates

U. Riebesell*, D. A. Wolf-Gladrow & V. Smetacek

Alfred Wegener Institute for Polar and Marine Research, D-2850 Bremerhaven, Germany

THE supply of dissolved inorganic carbon (DIC) is not considered to limit oceanic primary productivity[1], as its concentration in sea water exceeds that of other plant macronutrients such as nitrate and phosphate by two and three orders of magnitude, respectively. But the bulk of oceanic new production[2] and a major fraction of vertical carbon flux is mediated by a few diatom genera whose ability to use DIC components other than CO_2, which comprises <1% of total DIC[3], is unknown[4]. Here we show that under optimal light and nutrient conditions, diatom growth rate can in fact be limited by the supply of CO_2. The doubling in surface water pCO_2 levels since the last glaciation from 180 to 355 p.p.m.[5,6] could therefore have stimulated marine productivity, thereby increasing oceanic carbon sequestration by the biological pump.

Dissolved inorganic carbon in sea water exists in three interchangeable forms: CO_2, HCO_3^- and CO_3^{2-}. Despite its low concentration (0.5%–1% of DIC, corresponding to 10–15 μM CO_2 at pH 8.2), CO_2 is the main source of inorganic carbon for phytoplankton growth in the natural environment. This is indicated both by phytoplanktonic stable carbon isotope compositions, which show a strong inverse relationship with ambient CO_2 concentrations[7], and by high phytoplanktonic $\delta^{13}C$ values during diatom blooms, which indicate limitation of the rate of photosynthesis by diffusive CO_2 transport[8]. Whereas some microalgae tested can use bicarbonate[4], common marine diatoms use only dissolved CO_2 (ref. 9).

Uptake of inorganic carbon by a photosynthetically active cell leads to concentration gradients of CO_2, HCO_3^- and CO_3^{2-} in the surrounding medium which deviate from equilibrium. At steady state, CO_2 uptake is balanced by diffusion of CO_2 down the gradient to the cell surface and conversion of HCO_3^- to CO_2. Diffusional transport to the cell surface is dominated by molecular diffusion, because turbulent shear is insignificant at phytoplankton size scales that are small compared with the Kolmogorov length scale[10]. By combining the processes of CO_2 molecular diffusion and its conversion from bicarbonate[11], the transport equation for CO_2 reads

$$\frac{D}{r^2}\frac{\mathrm{d}}{\mathrm{d}r}\left(r^2\frac{\mathrm{d}c}{\mathrm{d}r}\right)+k'(c_\infty-c)=0 \qquad (1)$$

where D is the diffusivity of CO_2, c is the concentration as a function of the radial distance r from the centre of the cell, c_∞ is the concentration of the bulk medium, k' the rate constant for conversion of HCO_3^- to CO_2 ($k'=k_1[OH^-]+k_2$, where k_1 is the rate constant for direct formation of CO_2 from bicarbonate, $[OH^-]$ the hydroxyl ion concentration, and k_2 the rate constant for the formation of CO_2 from H_2CO_3). With $c(r\to\infty)=c_\infty$ and $c(r=a)=c_a$, a being the cell radius, integration of equation (1) yields

$$\frac{c-c_\infty}{c_a-c_\infty}=\frac{a}{r}\exp\left(\frac{a-r}{a_k}\right) \qquad (2)$$

where $a_k=\sqrt{D/k'}$. The total flux of CO_2 to the cell, Q_a, is then given by

$$Q_a=-4\pi a^2 D\frac{\mathrm{d}c}{\mathrm{d}r}=4\pi aD\left(1+\frac{a}{a_k}\right)(c_\infty-c_a) \qquad (3)$$

In equation (3), the quotient a/a_k represents the portion of Q_a contributed by conversion of CO_2 from HCO_3^-. This portion can be calculated for any given cell size, a, from the a_k values plotted in Fig. 1 as a function of pH and temperature. For a typical diatom, cell radius $a=15$ μm, the fraction of CO_2 supplied by conversion from HCO_3^- would lie between 15/300 (5%) and 15/800 (~2%) of the total CO_2 supply. Thus, as for other nutrients, the transport of CO_2 to the cell surface is predominantly by way of molecular diffusion.

Comparison of the CO_2 flux to the cell surface with the flux of nitrate and phosphate (calculated from equation (3)) yields a flux ratio of C/N/P which deviates significantly from the Redfield ratio. At nutrient concentrations typical of conditions at the onset of high-latitude phytoplankton spring blooms and

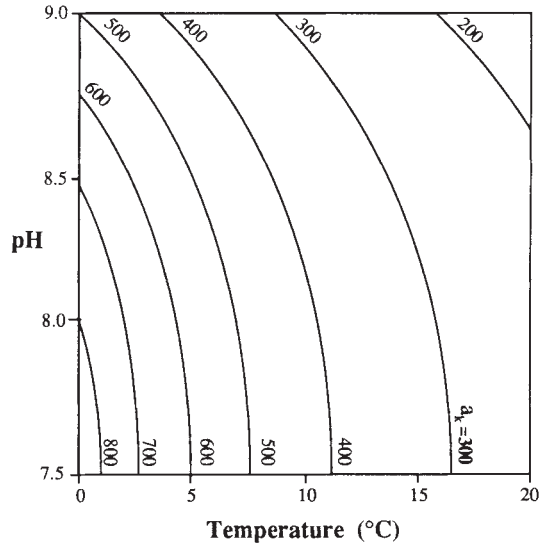

FIG. 1 Value of a_k (in μm) as function of pH and temperature; a/a_k provides the relative CO_2 supply to the cell from conversion of HCO_3^- to CO_2. HCO_3^- conversion becomes significant only for large cell sizes ($a>50$ μm) at high pH and temperature. At pH and temperature ranges generally observed in the ocean (pH 7.8–8.5; 0–20 °C), conversion of HCO_3^- to CO_2 contributes less than one-tenth of the total CO_2 supply to a typical phytoplankton cell ($a=5$–30 μm).

* Present address: Department of Biological Sciences, University of California, Santa Barbara, California 93106, USA.